Vibrational Properties of Hexagonal Boron Nitride: Inelastic X-Ray Scattering and *Ab Initio* Calculations

J. Serrano,[1,*] A. Bosak,[1] R. Arenal,[2] M. Krisch,[1] K. Watanabe,[3] T. Taniguchi,[3] H. Kanda,[3] A. Rubio,[4,5] and L. Wirtz[6,5]

[1]*European Synchrotron Radiation Facility, Boîte Postale 220, 38043 Grenoble, France*
[2]*Materials Sciences Division, Argonne National Laboratory, Argonne, Illinois 60439, USA*
[3]*National Institute for Materials Science, 1-1 Namiki, Tsukuba, 305-0044, Japan*
[4]*Departamento de Física de Materiales, Facultad de Ciencias Químicas, Universidad del País Vasco, Centro Mixto CSIC-UPV/EHU and Donostia International Physics Center, E-20018 San Sebastián, Basque Country, Spain*
[5]*European Theoretical Spectroscopy Facility (ETSF), E-20018 San Sebastián, Basque Country, Spain*
[6]*IEMN (CNRS-UMR 8520), Boîte Postale 60069, 59652 Villeneuve dAscq Cedex, France*

(Received 14 December 2006; published 1 March 2007)

The phonon dispersion relations of bulk hexagonal boron nitride have been determined from inelastic x-ray scattering measurements and analyzed by *ab initio* calculations. Experimental data and calculations show an outstanding agreement and reconcile the controversies raised by recent experimental data obtained by electron-energy loss spectroscopy and second-order Raman scattering.

DOI: 10.1103/PhysRevLett.98.095503 PACS numbers: 63.20.Dj, 61.10.Eq, 63.10.+a, 71.15.Mb

Besides their intermediate structure between two-dimensional sheets and 3D crystals, layered compounds are relevant materials for storage of other compounds [1] and as potential building blocks for nanotubes [2]. Among these materials, graphite and hexagonal boron nitride (*h*-BN) have drawn most of the attention due to their simple hexagonal structure, their fascinating properties, and the successful realization of carbon- [3] and more recently BN [4–6] nanotubes. A wide band gap semiconductor, *h*-BN, has been grown successfully very recently as a single crystal. It exhibits a lasing behavior at 5.8 eV that makes it attractive for optoelectronic applications in the ultraviolet energy range [7].

Despite the tremendous effort devoted to the characterization of physical properties of *h*-BN, the lattice dynamics, responsible for the elastic and thermodynamic properties such as the heat capacity and the thermal expansion, are still under debate. First principles calculations are generally accepted as the most accurate theoretical description of the lattice dynamics [8]. Recently, for *h*-BN, the validity of state of the art *ab initio* calculations was put in doubt by two experiments: Rokuta *et al.* [9] reported the only experimental data available for the phonon dispersion relations by electron-energy loss spectroscopy (EELS) performed on a monolayer of *h*-BN deposited on a Ni(111) substrate. Among several deviations from *ab initio* calculations of the lattice dynamics both for a monolayer [10,11] and for bulk *h*-BN [12,13], the EELS data show a degeneracy at the *K* point between acoustic (ZA) and optical (ZO) modes polarized along the *c* axis. The origin of this degeneracy has not been clarified yet. More recently [14], second-order Raman spectra of single crystalline *h*-BN revealed two features that contested the predictions based on a simple doubling of the energy scale of *ab initio* calculations for the one-phonon density of states, suggesting deviations up to 40% for the calculated energy of the TA branch in the *K*-*M* region. Since *h*-BN is a relevant material for UV lasing, it is imperative to resolve the existing controversies and critically assess the quality of the *ab initio* calculations. Furthermore, we need exact information on the lattice dynamics in order to properly understand the contributions due to electron-phonon coupling observed in the cathodoluminescence and absorption spectra of *h*-BN [7] and BN nanotubes [15,16].

In this Letter we address the above discrepancies in the vibrational properties by reporting inelastic x-ray scattering (IXS) measurements and first principles calculations of the phonon dispersion relations of bulk *h*-BN. We also report *ab initio* calculations of the phonon dispersion of a monolayer of *h*-BN on a nickel substrate. Our results and analysis yield a complete picture of the lattice dynamics of *h*-BN, reconcile theoretical and experimental data, and reveal the origin of the controversies raised by the EELS and Raman data.

Room temperature IXS measurements were conducted on beam line ID28 at the European Synchrotron Radiation Facility in Grenoble using *h*-BN single crystalline flakes of typical sizes of $500 \times 200 \times 50\ \mu\text{m}^3$ with the surface oriented perpendicular to the *c* axis. Monochromatic x rays of 17.794 and 15.817 keV were utilized to achieve an energy resolution of 3 and 5.5 meV, respectively. Furthermore, *ab initio* calculations were performed for the phonon dispersion relations and the eigenvectors using the ABINIT code [17,18], based on the linear response method [19] and within the local density approximation of density functional theory [20].

With 4 atoms in the unit cell and space group $P6_3/mmc$, *h*-BN phonon dispersion relations show 12 branches that can be divided into the $2E_{1u} + 2A_{2u} + 2E_{2g} + 2B_{1g}$ irreducible representations at the Brillouin zone center. The E_{1u} and A_{2u} are infrared active, the E_{2g} are Raman active, and the out-of-plane polarized B_{1g} modes, also denomi-

TABLE I. Experimental and calculated phonon energies (in meV) at the Γ point.

Symmetry	Experiment	Theory
E_{2g}	6.4[a]	6.5
B_{1g}(ZA)	silent	15.0
A_{2u}	97.1[b]	92.6
B_{1g}(ZO)	silent	100.4
E_{2g}	169.4[a], 169.9[c], 169.1[d]	171.0
E_{1u}(TO)	169.5[b]	170.9
E_{1u}(LO)	199.6[b]	199.7

[a]Raman data [21].
[b]Infrared data [22].
[c]Raman data [22].
[d]Raman data [14].

nated ZA and ZO modes, are silent. The acoustic modes have symmetry $E_{1u} + A_{2u}$ and the crystal field gives rise to a splitting between longitudinal (LO) and transverse optical phonons for the other E_{1u} modes, whereas the E_{2g} modes remain doubly degenerate each. In Table I we compare our calculations with the experimental data reported for the Γ point by Raman [14,21–24] and infrared [22,25] spectroscopy. The agreement between both data sets is excellent, the largest difference being a 5% underestimate of the A_{2u} mode, similar to that reported by previous *ab initio* calculations [12,13]. The high E_{2g} mode, marginally overestimated, is related via zone folding to the A_1 mode that dominates the Raman spectra of BN nanotubes [11,26].

Figure 1 displays selected IXS spectra of the TA modes along the [110] (Γ-*K*-*M*) direction, polarized along the *c* axis. The Stokes and anti-Stokes peaks are observed in the spectra taken at low momentum transfer *q* and a decrease of the intensity with increasing *q* is apparent. This mode exhibits a paraboliclike energy dependence at low *q*, typical for layered materials, and flattens towards the edge of the Brillouin zone, in excellent agreement with the calculated dispersion. The calculations predict the observation of the ZA acoustic branch only for (*q q L*) momentum transfers with odd *L*, in agreement with the upper branch in the inset of Fig. 1 obtained for $L = 3$ and with the absence of these modes in the displayed spectra, corresponding to momentum transfers with $L = 6$. The IXS data for the acoustic phonons has been employed for the determination of the five independent components of the elastic stiffness tensor of *h*-BN [27], providing an upper limit of 0.81 TPa for the axial elastic modulus of BN single-wall nanotubes, in agreement with several theories (0.85 TPa, [28,29]) and recent electric-field induced resonance experiments (0.722 TPa, [30]).

Figure 2(a) shows the experimental IXS phonon dispersions compared with the *ab initio* calculations (solid lines). The solid (open) circles correspond to modes polarized mainly along the *c* axis (in-plane) and Raman and infrared data are shown as open (green) and solid (magenta) diamonds, respectively. We shall emphasize the excellent

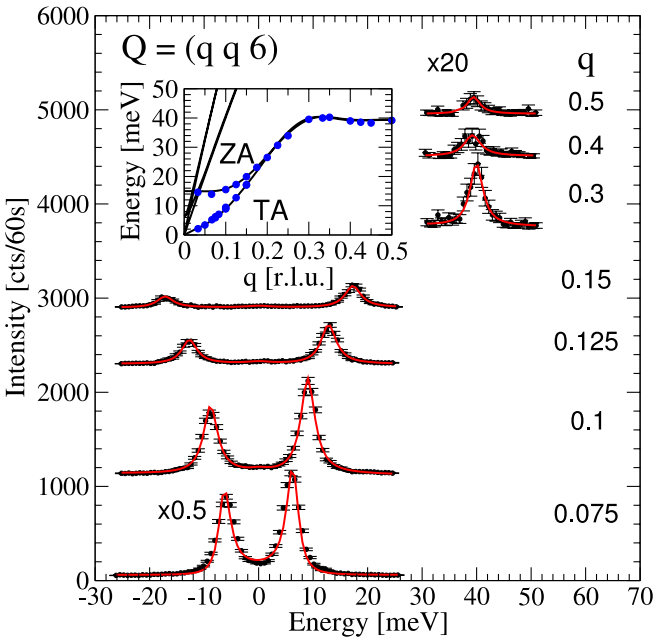

FIG. 1 (color online). Representative IXS spectra of *h*-BN for the TA branch along the [110] direction, polarized along the *c* axis. The symbols represent the IXS data whereas the solid (red) curves display the least-squares fit. The corresponding portion of the phonon dispersion is shown in the inset, where *q* is given in reciprocal lattice units (r.l.u.). The IXS data of the upper branch (ZA) were obtained for (*q q* 3) total momentum transfers.

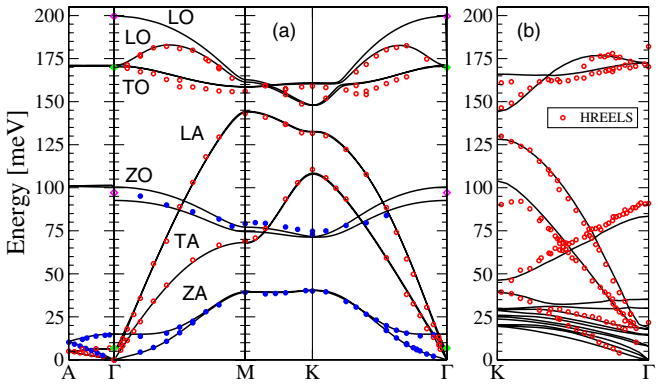

FIG. 2 (color online). (a) Phonon dispersion relations of *h*-BN along the main symmetry directions. The open (red) circles display modes polarized in the hexagonal plane whereas the solid (blue) circles correspond to modes polarized along the *c* axis. The solid curves represent the calculated phonon dispersion and infrared [22] and Raman [14,21,22] data at the Γ point are displayed by open (magenta) and solid (green) diamonds. (b) Calculated phonon dispersions of a monolayer of *h*-BN deposited on 3 layers of Ni (solid lines) compared to the EELS data from Ref. [9] (red open circles). Note that in the experiment only vibrational modes involving boron or nitrogen atoms were detected while in the calculations also the vibrational modes of the Ni substrate are included.

agreement between the calculated and IXS dispersions. Our calculations do not suffer from the negative energies displayed in Ref. [13] and reproduce the energy of the lowest lying Raman mode (shear mode) at 6.4 meV [21], improving upon those by Kern *et al.* [12]. This may be due to a combination of a larger energy cutoff for plane-wave expansion of the wave functions and the use of slightly larger lattice parameters [20]. Slight deviations occur for the high energy TO modes and amount to less than 3%, within the expected accuracy of this kind of calculations. Previous theoretical data [12,13] did not provide an accurate description of the quasiacoustic branches along the Γ-A direction.

The ZA-ZO splitting predicted by the theoretical models at the K point is well reproduced by the IXS data. Contrary to this, in the EELS measurements of Rokuta *et al.* [9] on a monolayer of h-BN deposited on a Ni(111) substrate, an almost degeneracy of ZA and ZO was found at K. We investigated two reasons that might lead to this almost degeneracy: (i) charge transfer from the h-BN monolayer to or from the substrate and (ii) the influence of the interlayer interaction with the substrate. As for the effect of charge transfer, we calculated the phonons for a charged single sheet of h-BN. Negative charging leads indeed to a closing of the gap between the ZA and ZO modes at K. However, a charging with 0.3 electrons per unit cell is necessary to reach degeneracy at K. This is in contrast to earlier calculations of the electronic structure of a single h-BN sheet on nickel where a transfer of 0.06 electrons to the substrate, i.e., a slightly positive charging of the sheet, was predicted [31]. We therefore conclude that charge transfer cannot be the origin of the degeneracy in the experiment of Rokuta *et al.* We performed an *ab initio* calculation of the phonon dispersion of a BN sheet on nickel to investigate the influence of the interaction with the substrate, simulated by three monolayers of Ni. The calculated dispersion and the EELS data are in excellent agreement, as displayed in Fig. 2(b). The differences between the EELS and IXS dispersions can therefore be attributed to the bonding between the h-BN monolayer and the Ni substrate. Indeed, the calculations of Grad *et al.* [31] had revealed a strong hybridization of the π orbitals of BN with the d levels of nickel, a polarization of the h-BN layer due to the substrate, and a substrate induced exchange splitting of electrons in the π band of h-BN. The π-d hybridization and a strong chemisorption have also been revealed by core electron and photoemission spectroscopies [32,33]. We can therefore conclude that the observed softening of the ZO branch stems from the binding of the layer to the substrate.

Figure 3 reproduces the second-order Raman spectrum of h-BN reported by S. Reich *et al.* in [14]. They compare their results with calculations of the one-phonon density of states (DOS) [12] for which the frequency scale has been multiplied by 2. This comparison implicitly assumes that

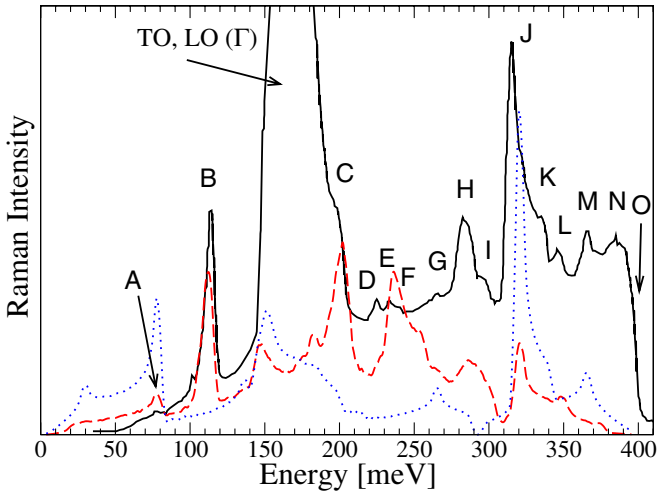

FIG. 3 (color online). Comparison of the second-order Raman spectrum of h-BN (solid, black) reported in Ref. [14] with our calculations for the one-phonon (dotted, blue line) and two-phonon (dashed, red line) DOS. The energy axis of the one-phonon DOS has been multiplied by a factor 2, in the same fashion as in Ref. [14]. The most relevant features of the experimental spectrum are labeled, and their energies compared with IXS data and calculations in Table II.

the overtones, i.e., sums of modes with the same frequency, are much stronger than combinations of phonons belonging to different branches. Although most of the spectral features are successfully assigned based on a detailed group theoretical analysis and the above assumption, the peaks found at 114 and 284 meV (labeled B and H in Fig. 3) were not compatible with the assignment. This led the authors to conclude that the calculated frequencies are too small to describe the spectra. The excellent agreement between IXS data and our calculations is in stark disagreement with this conclusion. The dotted (blue) line in Fig. 3 corresponds to our calculated one-phonon DOS scaled in the same way as the one used for comparison with the Raman data in Ref. [14]. The dashed (red) line, however, represents the full two-phonon DOS, taking into account both overtones and combinations. A wealth of new spectral features is obtained in this way and two of the strongest ones lie underneath the experimental features under discussion. In view of this agreement between the two-phonon DOS and the Raman spectra, we have analyzed the assignments of the other features and the result is summarized in Table II. Using the IXS data and the calculated dispersions, we therefore assign peaks B and H to combinations of ZA + ZO and LA + LO modes at the K point. Furthermore, the unknown peak reported at 2800 cm^{-1} (347.2 meV, labeled L) may be assigned to a combination of LO and TO modes at the overbending along the Γ-K and Γ-K-M directions. Beside these peaks, there is a general agreement with the assignments reported in [14], the discrepancies stemming from the explicit consideration of combination of modes with different frequency.

TABLE II. Experimental and calculated energies (in meV) for relevant features of the second-order Raman spectrum.

Label (Fig. 3)	Raman [14]	Assignment	IXS	Theory
A	76.9	2ZA(M)	78.8	78.8
B	114.1	ZA + ZO(K)	115.2	111.9
C	203.3	2ZO(Γ)		200.8
D	224.4	ZO + LA(M)	221.5	221.2
E	233.1	ZO + TO(K)	234.1	233.2
F	238.1	TA + LA(K)	242.1	240.7
G	265.3	TA + LO(K)	269.0	265.3
H	283.9	LA + LO(K)	289.9	286.9
I	300.0	LA + TO(M)	298.8	302.7
J	314.9	2TO(M-K)	317.8	320.5
K	338.5	2TO, 2LO(Γ)		341.8
L	347.2	LO + TO(overb.)	346.8	347.7
M	364.5	2LO(overb.)	364.7	365.5
N	378.2	LO + TO(Γ)		374.3
O	398.0	2LO(Γ)		399.4

In summary, we have reported the phonon dispersion relations of bulk h-BN obtained by IXS and *ab initio* calculations. The IXS data are in excellent agreement with the calculated dispersion and previously reported Raman and infrared data. The discrepancies observed between EELS and IXS data stem from the polarization of the h-BN monolayer due to the nickel substrate, a fact that poses a challenge in measurements of elastic and optical properties of BN nanotubes deposited on metallic substrates. The alleged discrepancies between calculations and second-order Raman spectral features disappear when one takes into account phonon combinations by calculating explicitly the two-phonon DOS.

We gratefully acknowledge F. J. Manjon, M. Muntwiller, and M. Hoesch for fruitful discussions. A. R. and L. W. acknowledge support by the European Community Network of Excellence Nanoquanta (No. NMP-CT-2004-500198). L. W. acknowledges funding by the French ANR and A. R. by the SANES project (No. NMP4-CT-2006-017310), Basque Country University, and MCyT. Calculations were performed at IDRIS and at the Barcelona Supercomputing Center.

*Electronic address: jserrano@esrf.fr

[1] M. S. Dresselhaus, G. Dresselhaus, K. Sugihara, I. L. Spain, and H. A. Goldberg, *Graphite Fibers and Filaments* (Springer-Verlag, Berlin, 1988).
[2] J. Nagamatsu *et al.*, Nature (London) **410**, 63 (2001).
[3] S. Ijima, Nature (London) **354**, 56 (1991).
[4] N. G. Chopra *et al.*, Science **269**, 966 (1995).
[5] R. S. Lee *et al.*, Phys. Rev. B **64**, 121405 (2001).
[6] R. Arenal *et al.*, Phys. Rev. Lett. **95**, 127601 (2005).
[7] K. Watanabe, T. Taniguchi, and H. Kanda, Nat. Mater. **3**, 404 (2004).
[8] S. Baroni *et al.*, Rev. Mod. Phys. **73**, 515 (2001).
[9] E. Rokuta *et al.*, Phys. Rev. Lett. **79**, 4609 (1997).
[10] L. Wirtz *et al.*, Phys. Rev. B **68**, 045425 (2003).
[11] L. Wirtz *et al.*, Phys. Rev. B **71**, 241402(R) (2005).
[12] G. Kern, G. Kresse, and J. Hafner, Phys. Rev. B **59**, 8551 (1999).
[13] W. J. Yu *et al.*, Phys. Rev. B **67**, 014108 (2003).
[14] S. Reich *et al.*, Phys. Rev. B **71**, 205201 (2005).
[15] B. Arnaud *et al.*, Phys. Rev. Lett. **96**, 026402 (2006).
[16] L. Wirtz, A. Marini, and A. Rubio, Phys. Rev. Lett. **96**, 126104 (2006).
[17] The ABINIT code is a common project of the Université Catholique de Louvain, Corning Incorporated, and other contributors (URL: http://www.abinit.org).
[18] X. Gonze *et al.*, Comput. Mater. Sci. **25**, 478 (2002).
[19] X. Gonze and C. Lee, Phys. Rev. B **55**, 10 355 (1997).
[20] The wave functions of valence electrons were expanded in plane waves with an energy cutoff of 40 a.u. Core electrons were replaced by Troullier-Martins pseudopotentials. A $9 \times 9 \times 4$ sampling was used for the integration over the Brillouin zone. Geometry optimization yielded an in-plane lattice constant of 2.496 Å and an interlayer distance of 3.254 Å. The dynamical matrix was calculated on a $14 \times 14 \times 6$ q grid and interpolated in reciprocal space for the calculation of phonons at an arbitrary phonon wave vector q.
[21] R. J. Nemanich, S. A. Solin, and R. M. Martin, Phys. Rev. B **23**, 6348 (1981).
[22] R. Geick, C. H. Perry, and G. Rupprecht, Phys. Rev. **146**, 543 (1966).
[23] T. Kuzuba *et al.*, Phys. Rev. B **18**, 4440 (1978).
[24] G. J. Exarhos and J. W. Schaaf, J. Appl. Phys. **69**, 2543 (1991).
[25] P. J. Gielisse *et al.*, Phys. Rev. **155**, 1039 (1967).
[26] R. Arenal *et al.*, Nano Lett. **6**, 1812 (2006).
[27] A. Bosak *et al.*, Phys. Rev. B **73**, 041402(R) (2006).
[28] E. Hernandez, Phys. Rev. Lett. **80**, 4502 (1998).
[29] K. N. Kudin, G. E. Scuseria, and B. I. Yakobson, Phys. Rev. B **64**, 235406 (2001).
[30] A. P. Suryavanshi *et al.*, Appl. Phys. Lett. **84**, 2527 (2004).
[31] G. B. Grad *et al.*, Phys. Rev. B **68**, 085404 (2003).
[32] A. B. Preobrajenski, A. S. Vinogradov, and N. Martensson, Phys. Rev. B **70**, 165404 (2004).
[33] A. B. Preobrajenski, A. S. Vinogradov, and N. Martensson, Surf. Sci. **582**, 21 (2005).